Database of 25 validated coil models for electric field simulations for TMS

Drakaki, Maria; Mathiesen, Claus; Siebner, Hartwig R.; Madsen, Kristoffer; Thielscher, Axel

Published in:
Brain Stimulation

Link to article, DOI:
10.1016/j.brs.2022.04.017

Publication date:
2022

Document Version
Publisher's PDF, also known as Version of record

Brain Stimulation 15 (2022) 697–706

Contents lists available at ScienceDirect

Brain Stimulation

journal homepage: http://www.journals.elsevier.com/brain-stimulation

Database of 25 validated coil models for electric field simulations for TMS

Maria Drakaki [a, b, c], Claus Mathiesen [b], Hartwig R. Siebner [c, d, e], Kristoffer Madsen [c, f, 1], Axel Thielscher [a, c, *, 1]

[a] Section for Magnetic Resonance, Department of Health Technology, Technical University of Denmark, Kgs, Lyngby, Denmark
[b] MagVenture A/S, Farum, Denmark
[c] Danish Research Centre for Magnetic Resonance, Centre for Functional and Diagnostic Imaging and Research, Copenhagen University Hospital Amager and Hvidovre, Copenhagen, Denmark
[d] Department of Neurology, Copenhagen University Hospital Frederiksberg and Bispebjerg, Copenhagen, Denmark
[e] Department for Clinical Medicine, Faculty of Medical and Health Sciences, University of Copenhagen, Copenhagen, Denmark
[f] Department of Applied Mathematics and Computer Science, Technical University of Denmark, Kgs Lyngby, Denmark

ARTICLE INFO

Article history:
Received 7 January 2022
Received in revised form
25 April 2022
Accepted 25 April 2022
Available online 28 April 2022

Keywords:
Transcranial magnetic stimulation
Electric field simulations
Coil models
Electric field properties
Motor threshold

ABSTRACT

Background: The effects of transcranial magnetic stimulation (TMS) on brain activity depend on the design of the stimulation coil. A wide range of coils from different vendors are currently used with different stimulation properties. This decreases the comparability of study results.
Objective: To systematically compare widely used commercial TMS coils concerning their focality, stimulation depth and efficacy. To provide validated models and data of these coils for accurate simulations of the induced electric fields.
Methods: We reconstructed the magnetic vector potential of 25 commercially available TMS coils of different vendors from measurements of their magnetic fields. Most coils had a figure-of-eight configuration. We employed the reconstructed magnetic vector potential in simulations of the electric field in a spherical head model. We estimated the motor thresholds of the coil-stimulator combinations using the calculated fields, the pulse waveforms and a leaky integrator model of the neural membrane.
Results: Our results confirm a previously reported systematic trade-off between focality and relative depth of stimulation. However, neither the peak field strength in the "cortex" of the sphere model nor the estimated motor thresholds were strongly related to the two former measures and need to be additionally determined.
Conclusion: Our comprehensive coil characterization facilitates objective comparisons of coils of different sizes and from different vendors. The models and auxiliary data will be made available for electric field simulations in SimNIBS. Our work will support TMS users making an informed selection of a suited coil for a specific application and will help to reduce uncertainty regarding the TMS-induced electric field in the brain target region.

1. Introduction

The coil geometry critically determines the spatial distribution of the electric field induced by transcranial magnetic stimulation (TMS) in the brain, together with the coil position and the ohmic conductivity distribution inside the head [1]. It can be optimized for specific applications such as a focal stimulation for motor mapping [2] or a stimulation of larger brain areas which might benefit therapeutic applications [3]. Dictated by the underlying physics (the Poisson equation), there are limitations to which electric field configurations can be achieved by TMS and well-known trade-offs between the electric field strength and the focality of the electric field [4–6]. For instance, coils that achieve a focal stimulation at the brain surface suffer from a very rapid decay of the electric field strength in deeper areas. Conversely, coils that stimulate also slightly deeper brain areas are necessarily

* Corresponding author. Danish Research Centre for Magnetic Resonance, Centre for Functional and Diagnostic Imaging and Research, Copenhagen University Hospital Amager and Hvidovre, Section 714, Kettegaard Allé 30, 2650, Hvidovre, Denmark.
E-mail address: axelt@drcmr.dk (A. Thielscher).
[1] These authors contributed equally to the work.

https://doi.org/10.1016/j.brs.2022.04.017

non-focal and thus, will strongly stimulate large regions on the brain surface.

Despite their practical relevance, the electric field distributions of commercial TMS coils have only been characterized in a few studies so far. The most comprehensive study revealed a systematic dependency between focality and depth decay both for figure-8 and round coils [4]. While these parameters are very useful, they do not capture all practically relevant properties of a coil-stimulator combination. Coils which score similar on both items can still be differently efficient in inducing neural activity and have different motor thresholds (MT) [7], but the underlying causes have so far not been fully described.

When aiming at quantitative dose comparisons, also the absolute strength of the TMS coil fields need to be accurately controlled. Up to now, most studies employed computational models that were derived from X-ray images or descriptions of the winding geometries supplied by the manufacturers [4,7,8]. Since the modelled and real geometries are likely to differ to some extent, it can be particularly challenging to accurately model the absolute strength of the induced electric field. Reconstructing theoretical coil models directly from measurements of the magnetic fields [9–11] can resolve this limitation, but the measurements are practically demanding and related studies have so far been limited to the demonstration and validation of the setup and approach rather than the characterization of several coils. Lastly, comparisons have been often limited to electric field distributions of TMS coils calculated for a fixed rate of change of the coil current. This disregards that the effect on the nerve membrane potential is also depending on the temporal shape of the TMS pulse and by that relies on the properties of both the coil and stimulator [12].

In this study, we set out to accurately characterize the electric fields of 25 commercial coil-stimulator combinations. Using a reconstruction method based on fitting magnetic dipoles [13], we determined the magnetic vector potential of each coil from three-dimensional measurements of its magnetic field distribution. We used the vector potential models to calculate focality, depth decay and the absolute electric field strength on the "cortical surface" in a spherical model of the head. Finally, the calculated fields were used together with the recorded pulse waveforms and a simple leaky integrator model of the neural membrane to estimate MT for the tested coil-stimulator combinations [14,15]. Applying an open-science framework, we hope that our work will become a valuable resource for TMS users assisting them in making optimal choices regarding the stimulation coil given their specific study aim.

2. Materials and methods

Fig. 1A provides an overview of the experimental workflow that was applied to each of the measured coils. The magnetic field distribution was acquired using an automated measurement setup (Fig. 1A) and used to reconstruct the magnetic vector potential [11,13]. The latter enabled the calculation of the electric field distribution in a spherical head model using SimNIBS (www.simnibs.org). The peak field strength on the "cortical" surface, the focality and the depth decay of the field were extracted from the simulated electric fields. Additional pickup coil measurements (Fig. 1B) were used to determine the pulse waveform and the induced voltage at maximum stimulator output (MSO). The data was used to calculate the maximal rate of change of the coil current dI/dt_{max}. Finally, the MT of the tested coil-stimulator combination was estimated from the previously determined parameters and a passive model of a nerve membrane.

2.1. Magnetic field measurements and reconstruction of magnetic vector potential distribution

The magnetic fields of 25 commercial TMS coils from four companies (Deymed, Mag&More, MagStim, MagVenture A/S) were measured at DRCMR, Copenhagen University Hospital Hvidovre, Denmark. Our aim was to include "standard sized" figure-8 coils of as many manufacturers as practically feasible during the time period of the study. If accessible, we measured also large figure-8 coils designed, e.g. for OCD treatment as well as small figure-8 coils aimed at motor mapping. Requests from SimNIBS users was another motivation to include specific coils, such as the MagVenture MRI-B91. For two coil types (MagVenture MCF-B65, MC-125), two versions were measured that differed in the type of litz wire due to a production update. As far as available from the homepages of the manufacturers, the technical coil parameters of the coils are listed in Table S1 for completeness.

The measurements were done in two successive steps. First, a purpose-built measurement setup (MagProbe, Skjøt Consulting Aps, Denmark) was used to determine the magnetic field of each coil for a current strength of 1A. The data was used to reconstruct the magnetic vector potential distribution for each coil for a fixed rate of change of 1A/s of the coil current. Second, additional pickup coil measurements were used to record the specific pulse waveform and the maximal stimulation strength for each of the 25 coil-stimulator combinations. This was used to determine the maximal rate of change dI/dt_{max} and estimate the MT for each coil-stimulator combination. The values of dI/dt_{max} are reported in units of A/μs (rather than A/s) for convenience.

The purpose-built measurement setup consists of a three-axis Hall probe (Honeywell HMC1043) placed inside a plastic rod that is moved in three dimensions by stepper motors (Fig. 1B). The setup drives the TMS coil with a 1 kHz sinusoidal current of fixed amplitude using a built-in function generator, and internally scales the measured magnetic field values to correspond to a current flow of 1A before saving them together with the measurement positions. The coil was placed on the acrylic glass surface of the measurement setup and the magnetic field was sampled in a volume extending beyond the coil by approximately 28 cm in both the x- and y-directions and covering approximately 24 cm in z-direction (depending on the coil thickness). According to the coil size, the sampling resolution was set to 6–8 mm along x- and y-directions. Resolution in z-direction was fixed to approximately 10 mm by the measurement software. A further measurement was performed to record the field directly above the coil surface at a higher resolution of 3–5 mm. The coil was turned on the other side and the measurements repeated. We verified that the results obtained for square test coils of known dimensions closely matched their theoretical magnetic field values with an error of less than 2%.

Three-dimensional distributions of the magnetic field and of the magnetic vector potential for a coil current of 1A were reconstructed from the measured magnetic fields using a dipole approximation, which offers improved flexibility to work with arbitrary winding geometries compared to our earlier reconstruction method [11]. The main advantage of this method is that it is applicable to arbitrary coil geometries, including highly curved coils, and requires only coarse knowledge of the positions of the coil windings. Briefly, the coils were modelled as dipole expansions according to positions gridded within a coarse representation of the coil volume (available as.stl files accompanying the coil models). For flat coils, these dipoles were restricted to one direction, whereas three orthogonal components were fitted for non-flat coils. Then, a L2-regularized minimum norm estimator was used to

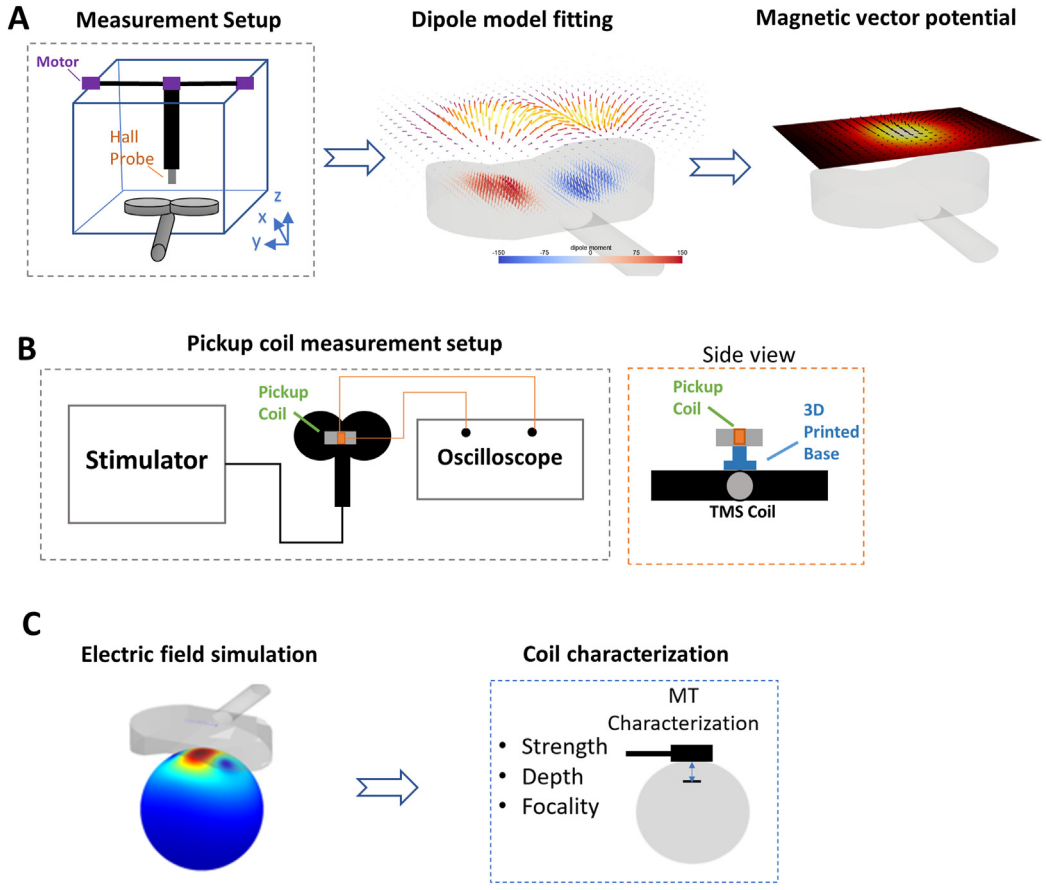

Fig. 1. TMS coil model creation and validation methods. A) Left: Schematic illustration of the custom-built measurement setup (maximal measurement volume: 400 mm × 400 mm x 240 mm in x-, y- and z-directions). Center: The data of the magnetic field measurements are exemplified by a plane of arrows above the coil. The data is used to fit a dipole expansion indicated by the red and blue arrows inside the coil casing. The dipole strength is indicated by the length of the arrows. The color (red vs. blue) indicates whether a dipole points along the positive or negative z-axis. Right: The magnetic vector potential as reconstructed from the dipole expansion is shown in a plane above the coil. The color scale indicates the magnitude of the magnetic vector potential and the arrows the direction. Note that the magnetic vector potential has only a weak component along the z-axis as the modelled figure-8 coil is mostly flat (MagVenture MC-B70). B) Measurement of the time course and strength of the stimulation pulse with a pickup coil positioned at the center of the TMS coil. This served to estimate the maximum *dI/dt* for each coil-stimulator combination and record the shape of the pulse waveforms. C) The coil model was used to determine the focality, depth decay and the peak electric field strength on the "cortex" layer of the spherical head model for a fixed *dI/dt* of 1A/μs. The coil model, the maximum *dI/dt* and the waveform was then used to estimate the motor threshold (MT) of the measured coil-stimulator combination. (For interpretation of the references to color in this figure legend, the reader is referred to the Web version of this article.)

fit the magnitudes of the dipoles to approximate the B field measurements. To avoid overfitting and ensure stability of the solutions, the L2 regularization parameters were determined by split-half cross validation considering both predictability and reliability (minimizing difference between parameters fitted for each split). The number of dipoles used to represent each coil is available in Table S2 for completeness. Once the dipole moments were fitted, the magnetic vector potential was calculated by superposition of the dipoles and then used as "coil models" for calculation of the induced electric fields, as detailed in the next section. The method is validated and described in further detail in Ref. [13].

In addition, circular pickup coils were used to record the pulse waveform and determine dI/dt_{max} at 100% MSO for each of the 25 coil-stimulator combinations using biphasic pulse types (stimulators: Deymed DuoMAG DM-XT 1101606 - SN: D0931606C, Mag&more PowerMag P-Stim 160 - SN: PST06002, MagStim Rapid – SN: ENG35, MagVenture MagPro X100 - SN: 1050 and MagPro XP – SN: 1002). Three different pickup coils, including one with a different diameter, were used to assess the stability of the recordings and prevent biases. Each was made of five thin wire loops (diameter: 20 mm for two coils, 29.6 mm for the third) and placed in a 3D-printed holder to ensure a fixed distance to the TMS coil surface. The pickup coils were positioned to get stable read-outs of the induced voltage (on top of the center of figure-8 coils; 25–30 mm from the center for round coils) and the pulse waveform at 100% MSO was recorded three times with each pickup coil using an oscilloscope (Teledyne Lecroy, Wavejet Touch 354) and averaged. The pulse width was derived from the averaged time course. In pretests, we additionally confirmed that the relationships between the pickup coil measurements and the stimulation strength in %MSO did not show practically relevant deviations from linearity, in line with an earlier report [16].

For determining dI/dt_{max} of each coil-stimulator combination, the reconstructed magnetic field (denoted by $\vec{B}$) was numerically integrated over the area of the pickup coil (denoted by A) to determine the voltage induced for a rate of change of 1A/s of the TMS coil current

$$U_{ind}\left(dI/dt = 1\,A/s\right) = N \cdot \iint_A \vec{B}\, d\vec{A} \Big/ s \,. \quad (1)$$

The number of wire loops for the pickup coils (N) was 5. Using the linear relationship between induced voltage and rate of change of the TMS coil current, dI/dt_{max} was then calculated as

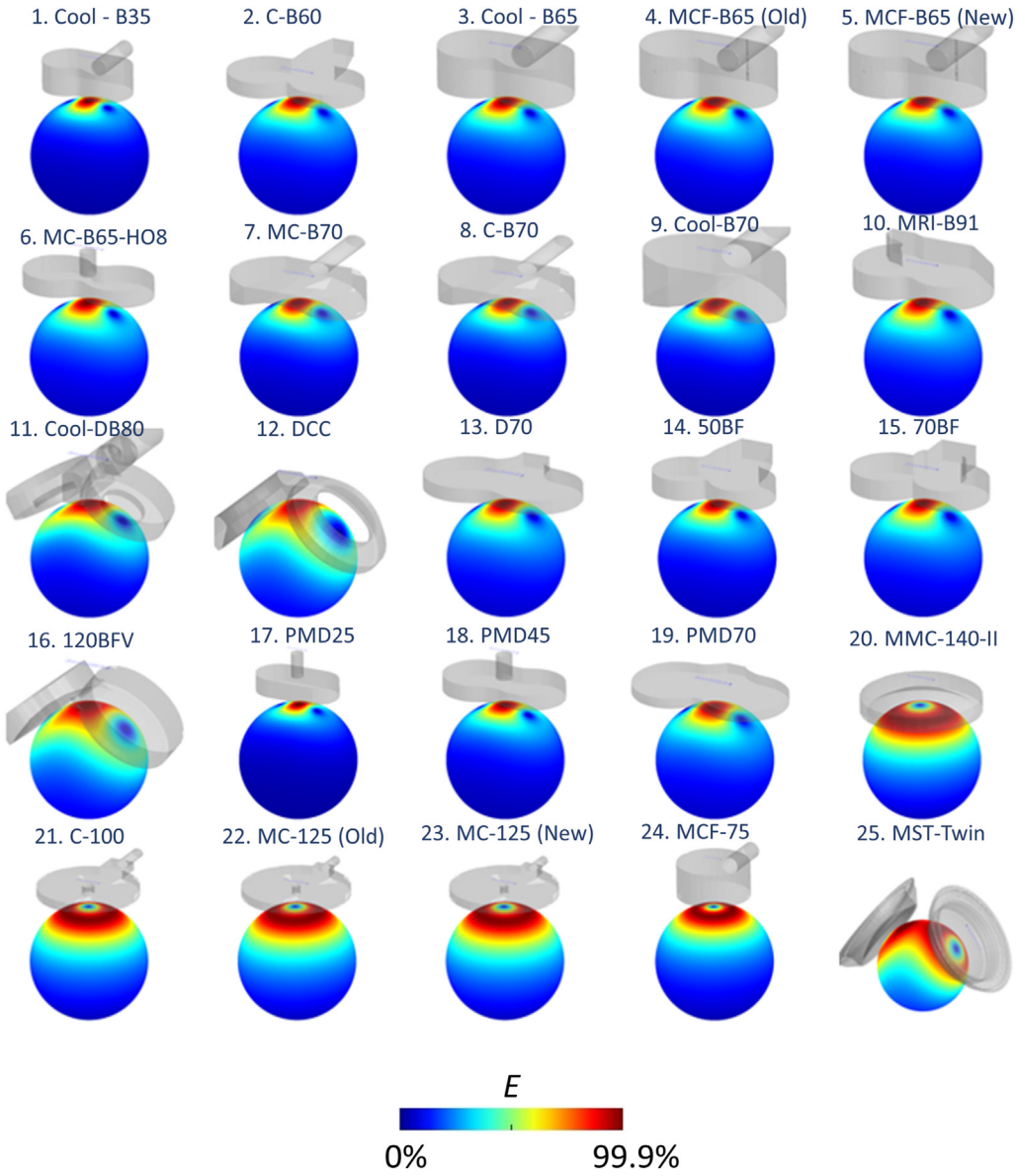

Fig. 2. Induced electric field distribution of 25 TMS coils. The simulations were conducted with SimNIBS software. The coil cases were created in Blender (https://www.blender.org/). All coils were placed at the center of the sphere head with directions as seen at the figure.

$$dI/dt_{max} = \frac{U_{ind}(100\%\ \mathrm{MSO})}{U_{ind}\left(dI/dt = 1\ A/s\right)}, \quad (2)$$

where $U_{ind}(100\%\ MSO)$ is the measured voltage induced in the pickup coil at 100% MSO. For convenience, the resulting value for dI/dt_{max} are reported in units of A/μs (rather than A/s) for further use. For the MagVenture coils, the dI/dt_{max} reported at the stimulator panel was also assessed.

2.2. Electric field simulations

The electric field induced in a homogenous spherical volume conductor (85 mm radius, conductivity 0.33S/m) was calculated for a dI/dt of 1A/μs using SimNIBS v.3.2.2 (www.simnibs.org) [17]. The volume conductor was selected to match the one used in a prior study [7] to enable a direct comparability of the results. It is worth noting that the electric field induced in a homogeneous sphere is not dependent on the conductivity [5], making this choice noncritical. The coils were positioned directly on top of it (Fig. 2). The cortex was assumed to be 15 mm below the outer surface. The peak electric field strength E_{max} on the cortex surface was determined. Additionally, it was confirmed that E_{max} did not correspond to putative outliers in the finite element simulations by comparing it with the 99.9% percentile of the field strength. Please note that the choice to calculate E_{max} for a rate of change of 1A/μs is arbitrary. However, as the ratio between the E_{max} of two coils is important for comparisons, this choice does not affect the interpretation of the results. In addition, as dI/dt_{max} is reported in units of A/μs, this choice is convenient as it allows for a simple multiplication of the values of E_{max} and dI/dt_{max} to get the peak electric field strength at 100% MSO of the stimulator.

Depth decay was characterized by the radial distance from the cortical surface to the deepest point where the electric field strength was half of E_{max}, denoted by $d_{1/2}$ in line with [7]. Focality was characterized by $S_{1/2} = V_{1/2}/d_{1/2}$, whereby $V_{1/2}$ indicates the

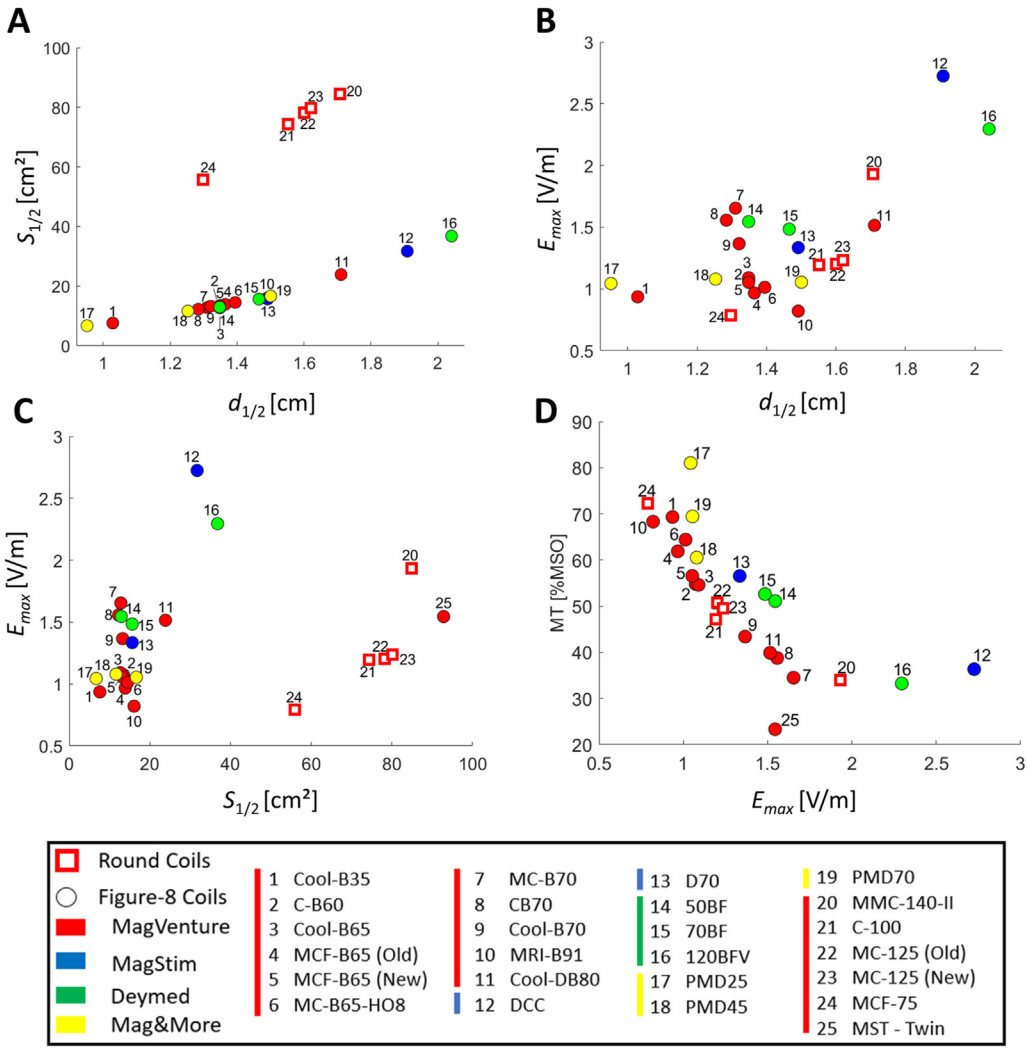

Fig. 3. Electric field characterization of 25 commercial TMS coils. A) Depth-focality tradeoff of the induced electric field. B) Peak strength of the electric field on the cortex surface plotted against the depth decay of the field. C) Peak strength of the electric field on the cortex surface plotted against the focality of the field. D) Calculated MT of each coil plotted against the peak strength of the electric field on the cortex. **Note**: The MST-Twin coil (#25) is not included in Fig. 3A and B in order to achieve a better representation of the rest of the results. It was simulated for an angle of 110°, for which is had a calculated focality of 92.8 cm^2 and a depth at half maximum of 2.41 cm.

volume inside the cortical surface where the electric field strength exceeds half of E_{max}. Smaller values indicate better focality. The above parameters E_{max}, $d_{1/2}$ and $S_{1/2}$ depend ***only on the coil design***, but are not influenced by the stimulator. On the other hand, the motor threshold (MT), which is another practically relevant parameter is additionally influenced by the technical properties of the stimulator. For this reason, we also estimated the MT of each ***coil-stimulator combination***, as detailed next.

2.3. Motor threshold estimation

The MT is inversely related to E_{max} of the coil, i.e. coils that induce stronger electric fields at the same dI/dt will have lower MTs. As MT is usually evaluated in percentage of the MSO of the stimulator, MT is inversely related to the MSO. The same coil will have a lower MT when connected to a stimulator that can deliver a higher MSO. The MSO together with the coil inductance determine dI/dt_{max}. Finally, MT also depends on the pulse duration and temporal shape, which determines how efficiently the induced field will change the membrane potential. The duration of a biphasic pulse mainly depends on the coil inductance and the capacitance of the stimulator [18]. To get a rough estimate of the MT of a coil-stimulator combination, the recorded waveform was first scaled so that the peak at the beginning of the pulse equaled 1. The normalized waveform was then multiplied by E_{max} to account for the efficacy of the coil. As E_{max} corresponds to the electric field induced for a rate of change of the coil current of 1A/μs, the result was further multiplied by dI/dt_{max} to account for the MSO of the stimulator. Finally, it was fed into a simple model of a passive leaky nerve membrane with a time constant τ of 190 μs [14,15,19], which effectively acts as temporal low-pass filter:

$$U_m(t) = E_{max} dI/dt_{max} \int_{t'=0}^{t} w(t') e^{-(t'-t)/\tau} dt' \quad (3)$$

The parameter $w(t)$ denotes the normalized waveform. The peak change of the membrane voltage $U_{m,max}$ over the course of the stimulation pulse was extracted to characterize the stimulation strength at the "neural" level at 100% MSO. Please note that the simple nerve membrane model does not incorporate information about the length of the stimulated neural structure nor its

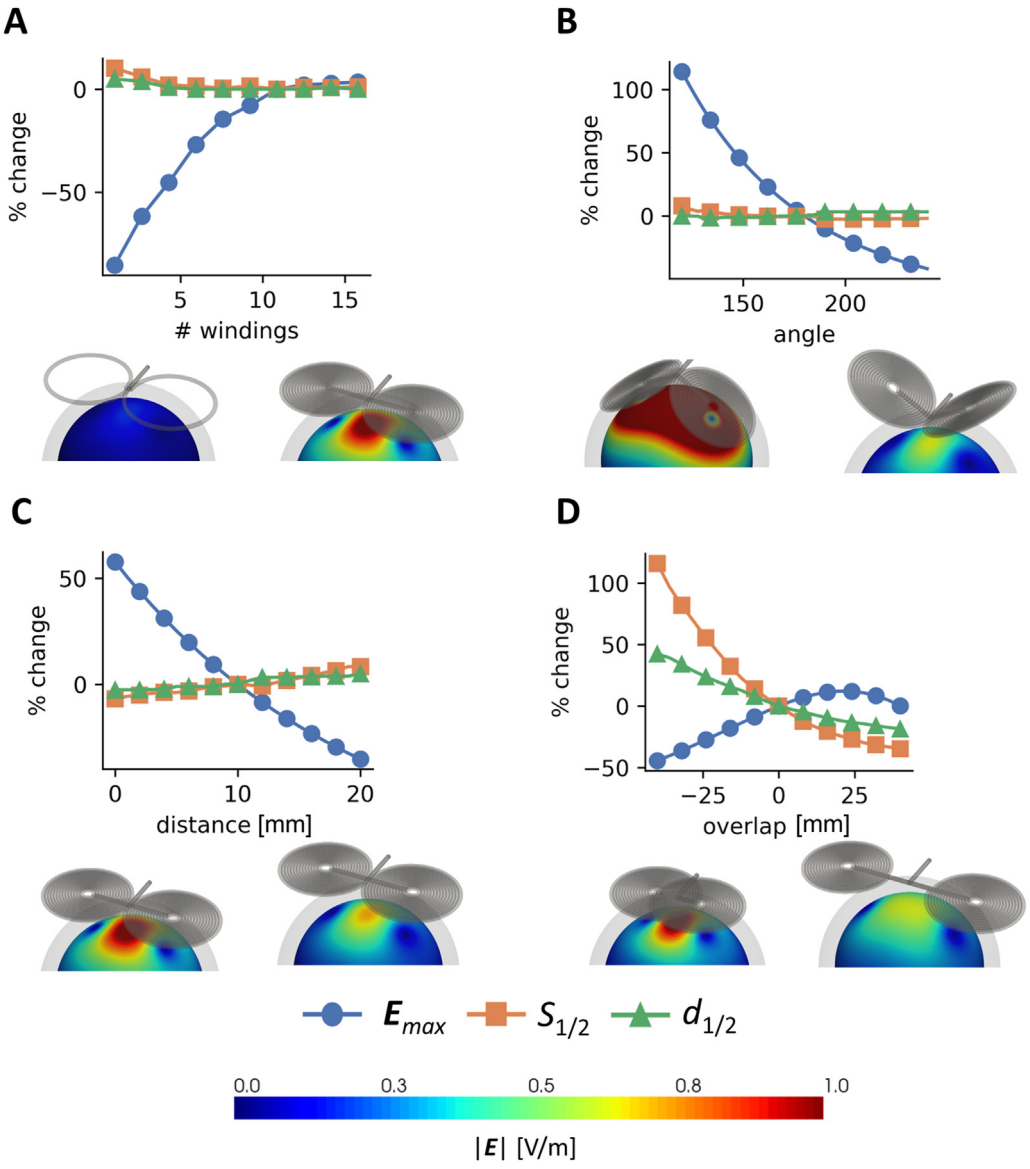

Fig. 4. Simulation a figure-8 coil when varying four selected technical parameters. For each of the cases, the parameters not being varied are fixed at their default values (outer winding diameter 80 mm, 14 coil windings, distance of 10 mm and the two coil wings directly next to each other). The peak electric field strength, focality and depth decay are measured relative to the default case, resulting a percentage scale. The results are also provided as an animation in the supplementary material. A) Changes in the peak electric field strength, focality and depth decay as a function of the number of coil windings. The illustrations below indicate the coil geometry and result of electrical field simulations for the extreme cases (1 and 16 coil windings). B) Simulations for variation of the angle between the coil wings, here the illustrated extreme cases are 120° and 240°. C) Simulations for different coil-to-"scalp" distances. The extreme cases are 0 mm and 20 mm. For commercial coils, different thicknesses of the casings on the side touching the head contribute to different coil-to-"scalp" distances. D) Simulations for varying overlap between the coil wings. The extreme cases are 40 mm overlap and a distance between the wings of 40 mm.

orientation relative to the electric field vector. Correspondingly, $U_m(t)$ and $U_{m,max}$ have units of V/m, indicating that they represent potential differences per unit length of the membrane. They are proportional to the change of the membrane potential of neural structures with the same time constant, so that the ratio between two $U_{m,max}$ is informative when comparing coil-stimulator combinations.

For estimating the MT, the "neural stimulation strength" $U_{m,max}$ of a biphasic pulse applied with a MagVenture MC-B70 figure-8 coil (coil #7 in the following results) was used as reference value. The average MT of the MagVenture MC-B70 figure-8 coil has been experimentally determined as 34.5% MSO for biphasic pulses [12]. This value was scaled with the ratio of the "neural stimulation strengths" to estimate the MTs of the other coil-stimulator combinations:

$$\mathrm{MT} = \frac{U_{m,max}(\mathrm{MC-B70})}{U_{m,max}}\mathrm{MT}_{\mathrm{MC-B70}} \quad (4)$$

In addition, to get insight into the accuracy of the calculated MTs, they were compared with experimentally determined MTs for a subgroup of coils for which MT measurements for biphasic pulses have been reported in literature.

2.4. Simulations based on parametric coil models

To allow a more principled investigation of how coil design parameters influence E_{max}, $d_{1/2}$ and $S_{1/2}$, we constructed a range of theoretical figure-8 coil models by systematically varying the number of windings, the angle between the two coil wings, the distance between the centers of the wings (overlap) and the coil-to-

Table 1
Estimated and experimentally measured MTs.

Nr	Manufacturer	Coil	MT estimated [% MSO]	MT literature [% MSO]	Muscle	Reference
1	MagVenture A/S	Cool-B35 (SN: 1019)	69.3	58.1	First dorsal interosseous (FDI)	Dubbioso et al., 2021 [29]
2	MagVenture A/S	C–B60 (SN: 1714)	54.3	50.7	Abductor pollicis brevis (APB)	Sundman et al., 2020 [30]
3	MagVenture A/S	Cool-B65 (SN: 2957)	51.7	59.7	First dorsal interosseous (FDI)	Davila-Pérez et al., 2018 [31]
7	MagVenture A/S	MC-B70 (SN: 1087)	34.5	34.5	Abductor pollicis brevis (APB)	Kammer et al., 2001 [12]
12	MagStim	DCC (SN: 233)	36.3	38.0	First dorsal interosseous (FDI)	Hardwick et al., 2014 [32]
13	MagStim	D70 (SN: 006)	55.1	50.3	Abductor pollicis brevis (APB)	Kammer et al., 2001 [12]
15	Deymed	70BF (SN: (21)47-6201111911E)	51.4	54.0	Abductor pollicis brevis (APB) & First dorsal interosseous (FDI)	Rens et al., 2021 [33]
17	Mag&More	PMD25 (SN: 02–2006)	81.0	63.1	First dorsal interosseous (FDI)	Allart et al., 2017 [34]
21	MagVenture A/S	C-100 (SN: 1017)	47.1	48.5	Abductor pollicis brevis (APB)	Hayashi et al., 2018 [35]
22	MagVenture A/S	MC-125 (SN: 1015)	50.5	47.0	First dorsal interosseous (FDI)	Cueva et al., 2016 [36]

cortex distance (corresponding to a varying thickness of the casing on the side touching the head). The current paths in the coils were modelled according to a spiral for each of the two coil wings, keeping the outer diameter fixed to 80 mm and assuming tight packing for a wire diameter of 5 mm. The two coil spirals were connected by strait wire segments to form a closed wire path, as depicted in the illustrations in Fig. 4. The coil models were used to calculate the electric field in the spherical head model for a rate of change of the coil current of 1A/ μs and derive E_{max}, $d_{1/2}$ and $S_{1/2}$. Briefly, first the magnetic vector potential for a line current along the coil wire path was solved, which was then used as input to calculations of the electric field using the finite-element method in SimNIBS. Further implementation details are given in paragraph S1 in the Supplementary Material.

3. Results

3.1. Focality, depth decay and induced electric field strength

Fig. 3A summarizes the relation between the focality and depth decay of the modelled coils. The results confirm the previously reported dependency between these two parameters and a generally higher focality of figure-8 compared to round coils [7]. Focality and depth decay can be related to the coil winding geometry: The most focal figure-8 coils with the steepest depth decay (#1–Cool-B35, #17–PMD25) have some of the smallest winding diameters as reported by the manufacturers. On the other hand, the least focal figure-8 coils with the flattest depth decay are large-diameter, curved coils (#12–DCC, #16–120BFV) and the MST-Twin coil with a calculated focality of 92.8 cm^2 and a depth at half maximum of 2.41 cm.

The peak electric field strength on the cortex differed up to factor 3 for the tested figure-8 coils and round coils (Fig. 3B). However, the relationship between the peak field strength on the cortex and the depth decay did not follow a clear pattern. For the figure-8 coils, there was a slight and expected tendency that less focal coils with a flatter depth decay also had a higher peak field strength. This was apparent when comparing two of the most unfocal coils (#12–DCC, #16–120BFV) with the rest. On the other hand, the three Mag&More coils (#17–PMD25, #18–PMD45-EEG, #19–PMD70) had relatively similar peak field strengths, but different depth decays.

Comparing peak field strength and focality for the figure-8 coils confirmed that the two most unfocal coils (#12–DCC, #16–120BFV) also had the highest peak field strengths (Fig. 3C). However, it also revealed that several coils with a similar focality in

Table 2
dI/dt_{max} and MT estimates. The experimentally determined MT of the MC-B70 was used as reference.

Nr	Manufacturer	Coil Model (serial #)	Pulse width [μs]	Calculated dI/dt_{max} [A/μs]	Stimulator dI/dt_{max} [A/μs]	MT [% MSO]
1	MagVenture A/S	Cool-B35 (SN: 1019)	315	141.3	145	69.3
2	MagVenture A/S	C–B60 (SN: 1714)	294	155.4	161	54.3
3	MagVenture A/S	Cool-B65 (SN: 2957)	299.5	149.8	155	51.7
4	MagVenture A/S	MCF-B65 (SN: 227)	302.5	147.9	151	61.0
5	MagVenture A/S	MCF-B65 (new litz wire; SN: 2434)	297	153.7	158	52.4
6	MagVenture A/S	MC-B65-HO8 (SN: 1)	337	129.0	124	64.4
7	MagVenture A/S	MC-B70 (SN: 1087)	303	155.3	151	34.5
8	MagVenture A/S	C–B70 (SN: 1116)	304	145.8	152	39.0
9	MagVenture A/S	Cool-B70 (SN: 2348)	308.5	143.8	146	43.4
10	MagVenture A/S	MRI-B91 (SN: 1075)	263.5	194.3	203	72.7
11	MagVenture A/S	Cool-DB80 (SN: 2178)	304.5	146.4	151	39.9
12	MagStim	DCC (SN: 233)	368.5	84.4	_	36.3
13	MagStim	D70 (SN: 006)	344.5	114.7	_	55.1
14	Deymed	50BF (SN: 47–6250131703)	336.8	97.6	_	50.0
15	Deymed	70BF (SN: (21)47-6201111911E)	327.8	101.1	_	51.4
16	Deymed	120BFV (SN: 47–6300251712F)	322	102.9	_	33.2
17	Mag&More	PMD25 (SN: 02–2006)	173	220.8	_	81.0
18	Mag&More	PMD45 (SN: 481400003)	174	249.6	_	60.5
19	Mag&More	PMD 70 (SN: 60)	165.5	241.3	_	68.7
20	MagVenture A/S	MMC-140-II (SN: 1287)	335.5	124.4	124	32.7
21	MagVenture A/S	C-100 (SN: 1017)	283.5	168.3	173	47.1
22	MagVenture A/S	MC-125 (SN: 1015)	291	151.7	163	50.5
23	MagVenture A/S	MC-125 (new litz wire; SN: 1508)	293.5	146.9	162	49.5
24	MagVenture A/S	MCF-75 (SN: 117)	291.5	160.0	163	73.0
25	MagVenture A/S	MST – Twin coil (SN: 1016) connected to MagPro XP (SN: 1002)	358.8	200.1	204	23.3

the range of 13–16 cm^2 differed by up to a factor 2 in the peak field strengths. In summary, while focality and depth decay are tightly related to each other and can be clearly linked to the coil winding geometry, this is not the case for the peak field strengths. The latter depends on further factors that are influenced by coil design choices, as demonstrated by the parametric simulation results shown next.

3.2. Dependence on coil design parameters

From the results of the parametric coil simulations in Fig. 4, it is obvious that most coil design parameters (angle, number of windings and distance) have a much stronger influence on the peak field strength than on the focality and depth decay. Only the dependence on the overlap between the two coil wings of the simulated figure-8 coil is similar for all three parameters. Therefore, there is substantial flexibility in designing a coil with similar focality and depth decay, but different peak field strength. This explains why E_{max} is only weakly linked to the two other parameters for the commercial coils.

3.3. MT and dI/dt_{max} estimation

Fig. 3D shows the relation between the estimated MT and the peak electric field strength. The expected inverse relationship is clearly apparent. In addition, coil-stimulator combinations from MagVenture tend to have lower MTs at similar E_{max} than the combinations of the other manufacturers. This reflects the additional dependence of MT on MSO and pulse width, both of which additionally depend on the stimulator rather than only the coil design. The correlation between our MT estimates and experimentally measured MTs collected from various studies (Table 1) was high (Pearson's $r = 0.83$), demonstrating that the MT estimates successfully captured the differences between the tested coil-stimulator combinations.

Table 2 lists the pulse width, dI/dt_{max} and the MT for every coil. The corresponding waveforms can be found in Fig. S1 of the Supplementary Material. The deviations of the estimated MT from a pure $1/E_{max}$ relationship in Fig. 3D demonstrates that the differences of the pulse width (range of 165.5–368.5μs) and dI/dt_{max} (range 84.4–249.6 A/μs) were large enough to clearly contribute to the different MTs of the tested coil-stimulator combinations. This is in line with the known dependence of MT on coil inductance, stimulator capacitance and the energy stored in the stimulator (these factors are not taken into account by E_{max}, but affect dI/dt_{max} and pulse width; e.g. Refs. [19,20]).

The median of the range of the dI/dt_{max} estimated across the three pickup coil measurements was 1.8% (maximum: 5.0%) across the 25 measured TMS coils. The maximum occurred for a round coil, for which the accurate positioning of the pickup coils was practically more difficult than for figure-8 coils. Comparison of the dI/dt_{max} estimated from the measurements and stated on the stimulator panel for the MagVenture coils revealed a relative difference of 2.9% (median) and 9.3% (maximum across all coils). We found a significant linear correlation between the difference and the pulse width (Pearson's $r = 0.6$; $p = 0.01$). After correcting for the linear dependency, the residual difference was 1.4% (median) and 5.9% (maximum). Based on additional controls (paragraph S2 in the Supplementary Material), we conclude that slight variations in the calibration of the dI/dt reported by the stimulator likely contributed to the observed differences to our pickup coil measurements. For the other stimulators, further validation of the estimated dI/dt_{max} was not possible as they do not report the realized dI/dt.

4. Discussion

We characterized the electric field properties of 25 different TMS coil-stimulator combinations. Majorly extending beyond prior studies, our work was based on measurements of the magnetic field distributions of the coils rather than theoretical models of the wire geometries [4,7,21], and included measurements of the strength and waveform of the TMS pulses. While our results support the previously reported relationship between focality and depth decay [4], neither the peak field strength nor the estimated MT were strongly related to them and should be additionally estimated. We employed a reconstruction approach which allowed us to derive theoretical coil models solely from the measured magnetic fields and coarse knowledge of the volume containing the coils wires. Our approach complements the findings of a prior study that experimentally determined key characteristics of 6 TMS coil types [22], but without the ability to reconstruct theoretical coil models from the experimental data. In contrast, the generic reconstruction approach used here allowed us to derive generally useable models of 25 coil types, which together with the measured pulse waveforms will be made publicly available [17] to enable quantitative comparisons of the stimulation "dose" of the tested coil-stimulator combinations.

4.1. Comparison of coil-stimulator combinations

Our results confirm a previously reported tradeoff between focality of the induced electric field and the steepness of the field decay with increasing depth [4]. Interestingly, these two metrics were only weakly related to the absolute electric field strength which the coils induced on the cortex for the same rate of change of coil current. A clear relation between peak field strength and focality was only apparent when comparing the two most unfocal figure-8 coils with the rest (#12–Magstim DCC, #16–Deymed 120BFV). Their size and curved design [23] both contribute to the high peak field strength. The relation was already less clear for the slightly more focal MagVenture Cool-DB80 coil, which had a lower peak field strength compared to some more focal coils. Due to the higher dI/dt_{max} of the MagVenture simulator, the three coils had similar MTs for a depth of 1.5 cm.

Parametrically varying selected design parameters (Fig. 4) confirmed that most of them had a stronger influence on the absolute electric field strength than on focality or depth decay. This shows that design differences of similarly sized commercial coils will lead to stronger differences in their peak field strength than in their focality or depth decay. MT depends mostly on the peak electric field strength, pulse waveform and the stimulator-specific maximal strength (cf. equation (3)&4). The waveform of a biphasic pulse is influenced by several parameters such as the capacitance of the stimulator, the coil inductance and the resistance of the stimulation circuit, indicating why also details such as the wire type influences the MT (see the two versions of the MagVenture MCF-B65, #4 vs #5). This explains why a large range of MTs from 34.5% to 68.3% was observed for several commonly used figure-8 coils which all share a similar "medium" focality of 13–16 cm^2. However, as the commercial coil-stimulator combinations differ in several parameters at the same time, it is not possible to attribute the observed differences in the electric field strength and MT to a single factor. This becomes apparent when comparing two medium focality coils of the same company with very different electric field strengths and MTs (MagVenture MC-B70 vs. MRI-B91, #7 vs #10): These coils differ in the amount of overlap between the wings (only the MC-B70 has an overlap), the number windings (10 vs 8), the casing thickness (due to the intended use in the MR scanner, the casing is more robust for the MRI-B91 and the wires

are further inside) and the inductance (apparent from the different pulse width of 303 vs 264 μs).

Differences in the peak electric field strength and MT are relevant, as a high estimated MT points towards a limited flexibility for practical applications, e.g. when encountering subjects with high individual MTs or aiming to place EEG electrodes underneath the TMS coil. Low MTs in combination with a flat depth decay are also advantageous when aiming for deeper cortical targets, as potentially useful in some clinical applications [3]. This is in contrast to, e.g. motor mapping [2] where high focality is more relevant to reach good spatial resolution. Unless cooling is used, higher MTs usually also come at the cost of faster heating in repetitive TMS protocols.

4.2. Comparison with existing models of the same coil types

Compared to the model of the MagVenture MC-B70 coil that is already included in SimNIBS [7], the new model has a difference of 4.3% for the peak electric field strength and 2.9% for depth and 4.1% for focality. For the models of the Magstim D70 coil, the differences in the peak field strength were 10.4%, while they were 2.3% and 2% for depth and focality. Comparing our models (#2–C-B60, #7–MC-B70, #12–DCC, #13–D70) with models that were added to SimNIBS according to geometrical information provided by Deng et al. [4] (https://github.com/simnibs/simnibs-coils) revealed maximal and median differences in the peak electric field strength of 23.3% and 10.8%, which were higher than the corresponding differences for the depth decay (maximal: 4.7%, median: 2.8%) and the focality (maximal: 12.9%, median: 6.8%). These comparisons confirm that it seems generally more straightforward to estimate focality and depth decay from coil models, and that ensuring a good correspondence between the modelled and real peak field can be more challenging when having only geometric information about the coil windings available. This is in line with the results of the parametric coil simulations (Fig. 4) which showed that many coil parameters (and putative inaccuracies of the theoretical coil models in those parameters) will have a stronger influence on the modelled absolute electric field strength than on the relative field distribution.

4.3. Strength and limitations

Our study was based on real measurements of the magnetic field distributions of the coils rather than merely theoretical information of the wire geometries and it additionally included measurements of the intensity and waveform of the TMS pulses. This enabled us to accurately determine the absolute strength of the coil fields, which is more difficult to ensure when using theoretical models only. In addition, the data allowed us to estimate the motor threshold of the tested coil-stimulator combinations, which is a practically highly relevant parameter.

Our study also has some limitations. The employed spherical volume conductor only coarsely mimics the real conductivity distribution inside the human head. Similarly, the passive nerve model is a simplification of the morphologically and electrophysiologically complex cortical neurons. These models were appropriate for the purpose of our study to characterize the general impact of different coil geometries and waveforms on the efficiency of stimulation. However, they would not be suited for more advanced purposes such as explaining the well-known MT differences for varying coil orientations (e.g. Ref. [24]).

We have estimated the dI/dt_{max} and MTs only for biphasic stimulators due to limited access to stimulator hardware and resource limitations in the project. We have focused on biphasic stimulators, as they are currently most relevant from a clinical perspective. The MT was only estimated for a small hand muscle and the optimal coil orientation. While the correlation between estimated and measured MTs (Table 1) was good, MTs differ substantially depending on the coil orientation and the targeted body representation [25]. Differences between the estimated MTs and those reported in experimental studies are therefore expected.

We only tested specific samples of the different TMS coil types. While it is difficult to estimate the extent of manufacturing variations which likely also differ between coil types, prior results indicate that they are small in general [22]. Our results are also affected by the accuracy and precision of our measurement and reconstruction approach. Thus, we aimed to tightly control all steps of our approach using validation measurements for the 3D measurement setup, repeated measures using different pickup coils and a comprehensive validation of our reconstruction approach [11]. For the tested MagVenture coils, the comparison of the estimated dI/dt_{max} and the dI/dt_{max} stated on the stimulator panel served as control of the measurement accuracy, revealing a good correspondence (median residual difference of 1.4%, maximum residual difference of 5.9%). This error level reflects the combined inaccuracies of the Hall probe measurements, the reconstruction approach and the pickup coil measurements. We can expect that the error levels of the coil models (i.e. the reconstructed magnetic vector potentials) do not exceed this range. Specifically, converting between %MSO and dI/dt by using the dI/dt_{max} listed in Table 2 ensures that the calculated field strength is scaled according to the voltages measured by the pickup coils, which were very reliable and gave only small differences between the pickup coils.

5. Conclusion

Our comprehensive comparison of 25 different coil-stimulator combinations will facilitate the comparison of stimulation parameters between experimental studies using different equipment. In particular, the coil models will be made publicly available via SimNIBS (www.simnibs.org) and, together with the estimated dI/dt_{max} reported here, can help to improve the accuracy of quantitative estimations and comparisons of the distribution and strength of the induced electric fields. We used pulse waveforms and a simple neural model to extend our evaluation beyond the spatial properties of the induced electric field and estimate the MT. We hope that providing our comprehensive dataset as public resource will facilitate personalized simulations of the induced electric field [17] and the resulting effects on neural structures [26–28].

Declaration of interest statement

Hartwig Roman Siebner has received honoraria as speaker from Sanofi Genzyme, Denmark and Novartis, Denmark, as consultant from Sanofi Genzyme, Denmark, Lophora, Denmark, and Lundbeck AS, Denmark, and as editor-in-chief (Neuroimage Clinical) and senior editor (NeuroImage) from Elsevier Publishers, Amsterdam, The Netherlands. He has received royalties as book editor from Springer Publishers, Stuttgart, Germany and from Gyldendal Publishers, Copenhagen, Denmark. Maria Drakaki and Claus Mathiesen are employed at MagVenture A/S (Farum, Denmark). The other authors report no conflicts of interests.

CRediT authorship contribution statement

Maria Drakaki: Conceptualization, Methodology, Software, Validation, Investigation, Interpretation of results, Writing – original draft, Visualization. **Claus Mathiesen:** Resources, Conceptualization, Interpretation of results, Writing – review & editing, Supervision, Funding acquisition. **Hartwig R. Siebner:** Resources, Interpretation of results, Writing – review & editing, Supervision.

Kristoffer Madsen: Conceptualization, Methodology, Software, Investigation, Interpretation of results, Writing – original draft, Writing – review & editing, Supervision. **Axel Thielscher:** Conceptualization, Methodology, Software, Investigation, Interpretation of results, Writing – original draft, Writing – review & editing, Supervision, Funding acquisition.

Acknowledgements

This study was supported by the Innovation Fund Denmark (grant 7038-00163B) and the Lundbeck Foundation (grant R313-2019-622). HRS holds a 5-year professorship in precision medicine at the Faculty of Health Sciences and Medicine, University of Copenhagen which is sponsored by the Lundbeck Foundation (grant R186-2015-2138). We thank Brainbox Ltd (brainbox-neuro.com) for providing the tested Deymed equipment, and Mark Schram Christensen (Copenhagen University) for providing the tested Magstim coils.

Appendix A. Supplementary data

Supplementary data to this article can be found online at https://doi.org/10.1016/j.brs.2022.04.017.

References

[1] Thielscher A, Opitz A, Windhoff M. Impact of the gyral geometry on the electric field induced by transcranial magnetic stimulation. Neuroimage 2011;54:234–43. https://doi.org/10.1016/j.neuroimage.2010.07.061.
[2] Raffin E, Pellegrino G, Di Lazzaro V, Thielscher A, Siebner HR. Bringing transcranial mapping into shape: sulcus-aligned mapping captures motor somatotopy in human primary motor hand area. Neuroimage 2015;120:164–75. https://doi.org/10.1016/j.neuroimage.2015.07.024.
[3] Harel EV, Rabany L, Deutsch L, Bloch Y, Zangen A, Levkovitz Y. H-coil repetitive transcranial magnetic stimulation for treatment resistant major depressive disorder: an 18-week continuation safety and feasibility study. World J Biol Psychiatr 2014;15:298–306.
[4] De Deng Z, Lisanby SH, Peterchev AV. Electric field depth-focality tradeoff in transcranial magnetic stimulation: simulation comparison of 50 coil designs. Brain Stimul 2013;6:1–13. https://doi.org/10.1016/j.brs.2012.02.005.
[5] Heller L, van Hulsteyn DB. Brain stimulation using electromagnetic sources: theoretical aspects. Biophys J 1992;63:129–38. https://doi.org/10.1016/S0006-3495(92)81587-4.
[6] Deng Z-D, Lisanby SH, Peterchev AV. Coil design considerations for deep transcranial magnetic stimulation. Clin Neurophysiol 2014;125:1202–12. https://doi.org/10.1016/j.clinph.2013.11.038.
[7] Thielscher A, Kammer T. Electric field properties of two commercial figure-8 coils in TMS: calculation of focality and efficiency. Clin Neurophysiol 2004;115:1697–708. https://doi.org/10.1016/j.clinph.2004.02.019.
[8] Thielscher A, Kammer T. Linking physics with physiology in TMS: a sphere field model to determine the cortical stimulation site in TMS. Neuroimage 2002;17:1117–30.
[9] Petrov PI, Mandija S, Sommer IEC, Van Den Berg CAT, Neggers SFW. How much detail is needed in modeling a transcranial magnetic stimulation figure-8 coil: measurements and brain simulations. PLoS One 2017;12:1–20. https://doi.org/10.1371/journal.pone.0178952.
[10] Bohning DE, Pecheny AP, Epstein CM, Speer AM, Vincent DJ, Dannels W, et al. Mapping transcranial magnetic stimulation (TMS) fields in vivo with MRI. Neuroreport 1997;8:2535–8. https://doi.org/10.1097/00001756-199707280-00023.
[11] Madsen KH, Ewald L, Siebner HR, Thielscher A. Transcranial magnetic stimulation: an automated procedure to obtain coil-specific models for field calculations. Brain Stimul 2015;8:1205–8. https://doi.org/10.1016/j.brs.2015.07.035.
[12] Kammer T, Beck S, Thielscher A, Laubis-Herrmann U, Topka H. Motor thresholds in humans: a transcranial magnetic stimulation study comparing different pulse waveforms, current directions and stimulator types. Clin Neurophysiol 2001;112:250–8. https://doi.org/10.1016/S1388-2457(00)00513-7.
[13] Madsen KH, Drakaki M, Thielscher A. Electric field models of transcranial magnetic stimulation coils with arbitrary geometries: reconstruction from incomplete magnetic field measurements. ArXiv Prepr n.d.;arXiv:2112.
[14] Barker AT, Garnham CW, Freeston IL. Magnetic nerve stimulation: the effect of waveform on efficiency, determination of neural membrane time constants and the measurement of stimulator output. Electroencephalogr Clin Neurophysiol Suppl 1991;43:227–37.
[15] Peterchev AV, Goetz SM, Westin GG, Luber B, Lisanby S. Pulse width dependence of motor threshold and input–output curve characterized with controllable pulse parameter transcranial magnetic stimulation. Clin Neurophysiol 2013;124:1364–72.
[16] Koponen LM, Goetz SM, Peterchev AV. Sound comparison of seven TMS coils at matched simulation strength. Brain Stimul 2020;13:873–80.
[17] Thielscher A, Antunes A, Saturnino GB. Field modeling for transcranial magnetic stimulation: a useful tool to understand the physiological effects of TMS? Proc Annu Int Conf IEEE Eng Med Biol Soc EMBS 2015. https://doi.org/10.1109/EMBC.2015.7318340. 2015-Novem:222–5.
[18] Ilmoniemi RJ, Ruohonen J, Karhu J. Transcranial magnetic stimulation - a new tool for functional imaging of the brain. Crit Rev Biomed Eng 1999;27:241–84.
[19] Davey K, Epstein CM. Magnetic stimulation coil and circuit design. IEEE Trans Biomed Eng 2000;47:1493–9. https://doi.org/10.1109/10.880101.
[20] Gomez LJ, Goetz SM, Peterchev AV. Design of transcranial magnetic stimulation coils with optimal trade-off between depth, focality, and energy. J Neural Eng 2018;15:046033. https://doi.org/10.1088/1741-2552/aac967.
[21] Çan MK, Laakso I, Nieminen JO, Murakami T, Ugawa Y. Coil model comparison for cerebellar transcranial magnetic stimulation. Biomed Phys Eng Express 2019;5. https://doi.org/10.1088/2057-1976/aaee5b.
[22] Nieminen JO, Koponen LM, Ilmoniemi RJ. Experimental characterization of the electric field distribution induced by TMS devices. Brain Stimul 2015;8:582–9.
[23] Koponen LM, Nieminen JO, Ilmoniemi RJ. Minimum-energy coils for transcranial magnetic stimulation: application to focal stimulation. Brain Stimul 2015;8:124–34. https://doi.org/10.1016/j.brs.2014.10.002.
[24] Bungert A, Antunes A, Espenhahn S, Thielscher A. Where does TMS stimulate the motor cortex ? combining electrophysiological measurements and realistic field estimates to reveal the affected cortex position. Cerebr Cortex 2016:1–12. https://doi.org/10.1093/cercor/bhw292.
[25] Kesar TM, Stinear JW, Wolf SL, Sciences E, Zealand N, Rehabilitation N, et al. The use of transcranial magnetic stimulation to evaluate cortical excitability of lower limb musculature: challenges and opportunities. Restor Neurol Neurosci 2018;36:333–48. https://doi.org/10.3233/RNN-170801. The.
[26] Aberra AS, Wang B, Grill WM, Peterchev AV. Brain Stimulation Simulation of transcranial magnetic stimulation in head model with morphologically-realistic cortical neurons. Brain Stimul 2020;13:175–89. https://doi.org/10.1016/j.brs.2019.10.002.
[27] Salvador R, Silva S, Basser PJ, Miranda PC. Determining which mechanisms lead to activation in the motor cortex: a modeling study of transcranial magnetic stimulation using realistic stimulus waveforms and sulcal geometry. Clin Neurophysiol 2011;122:748–58. https://doi.org/10.1016/j.clinph.2010.09.022.
[28] Seo H, Schaworonkow N, Jun SC, Triesch J. A multi-scale computational model of the effects of TMS on motor cortex. F1000Research 2016;5:1945. https://doi.org/10.12688/f1000research.9277.3.
[29] Dubbioso R, Madsen KH, Thielscher A, Siebner HR. The myelin content of the human precentral hand knob reflects interindividual differences in manual motor control at the physiological and behavioral level. J Neurosci 2021;41:3163–79.
[30] Sundman MH, Lim K, Ton That V, Mizell J-M, Ugonna C, Rodriguez R, et al. Transcranial magnetic stimulation reveals diminished homoeostatic metaplasticity in cognitively impaired adults. Brain Commun 2020;2:1–15. https://doi.org/10.1093/braincomms/fcaa203.
[31] Davila-Pérez P, Jannati A, Fried PJ, Cudeiro Mazaira J, Pascual-Leone A. The effects of waveform and current direction on the efficacy and test–retest reliability of transcranial magnetic stimulation. Neuroscience 2018;393:97–109. https://doi.org/10.1016/j.neuroscience.2018.09.044.
[32] Hardwick RM, Lesage E, Miall RC. Cerebellar transcranial magnetic stimulation: the role of coil geometry and tissue depth. Brain Stimul 2014;7:643–9. https://doi.org/10.1016/j.brs.2014.04.009.
[33] Rens G, Orban de Xivry JJ, Davare M, van Polanen V. Motor resonance is modulated by an object's weight distribution. Neuropsychologia 2021;156. https://doi.org/10.1016/j.neuropsychologia.2021.107836.
[34] Allart E, Delval A, Caux-Dedeystere A, Labreuche J, Viard R, Lopes R, et al. Parietomotor connectivity in the contralesional hemisphere after stroke: a paired-pulse TMS study. Clin Neurophysiol 2017;128:707–15. https://doi.org/10.1016/j.clinph.2017.02.016.
[35] Hayashi CY, Neville IS, Rodrigues PA, Galhardoni R, Brunoni AR, Zaninotto AL, et al. Altered intracortical inhibition in chronic traumatic diffuse axonal injury. Front Neurol 2018;9:1–8. https://doi.org/10.3389/fneur.2018.00189.
[36] Cueva AS, Galhardoni R, Cury RG, Parravano DC, Correa G, Araujo H, et al. Normative data of cortical excitability measurements obtained by transcranial magnetic stimulation in healthy subjects. Neurophysiol Clin 2016;46:43–51. https://doi.org/10.1016/j.neucli.2015.12.003.